

Intralayer antiferromagnetism in two-dimensional van der Waals magnet Fe_3GeTe_2

Neesha Yadav, Shivani Kumawat, Sandeep, Brajesh Kumar Mani, and Pintu Das*

Department of Physics, Indian Institute of Technology, Delhi, Hauz Khas, New Delhi, India - 110016

(Dated: December 9, 2025)

For the van der Waals magnet Fe_3GeTe_2 , although a ferromagnetic ground state has been reported, there are also reports of complex magnetic behavior suggesting coexistence of ferromagnetism and antiferromagnetism due to the intricate interaction between Fe^{+3} and Fe^{+2} ions in this system. The exact nature of the interactions and the origin of antiferromagnetism are still under debate. Here, we report the observation of signature of ferromagnetic and antiferromagnetic couplings between different Fe-ions in the anomalous Hall effect measured for devices of mechanically exfoliated Fe_3GeTe_2 nano-flakes of thicknesses ranging from ~ 15 -20 layers. The temperature-dependent anomalous Hall effect data reveal two sharp step-like switchings at low temperature ($T \lesssim 150$ K). Our detailed analyses suggest the step-like sharp switchings in anomalous Hall resistance are due to the magnetization reversal behavior of different Fe-ions in individual layers of Fe_3GeTe_2 . The experimental results can be explained by considering an intra-layer antiferromagnetic coupling between Fe^{+3} and Fe^{+2} ions, whereas intra-layer ferromagnetic coupling between Fe^{+3} and Fe^{+2} in the system. Our experimental results and the analyses are supported by the first-principles calculations for energetics and intralayer as well as interlayer exchange coupling constants.

I. INTRODUCTION

The discovery of long-range magnetic order in two-dimensional van der Waals (vdW) magnets has opened up possibilities to explore fundamental questions, as well as for applications in future energy-efficient miniaturized spintronic devices. A strong anisotropy, which is a prerequisite for long-range order in lower dimensions, leads to the opening of an energy gap in the spin wave excitation as well as suppression of thermal fluctuations. Two-dimensional magnets, such as transition metal (TM) halides, TM-chalcogenides, and Fe_3GeTe_2 (FGT-3), exhibit a multitude of layered-dependent properties. However, due to the stability of FGT-3, etc., in air and the possibility of raising the T_C to about room temperature [1], this class of materials has attracted significant attention from researchers in recent years. FGT-3 shows itinerant ferromagnetic behavior due to Fe^{+3} ions and localized behavior due to Fe^{+2} ions [2]. The itinerant nature leading to the interplay of charge and spin degrees of freedom in the system makes it an excellent candidate for applications in spintronics. New properties are being explored by the formation of heterostructures using FGT-3 with other relevant materials. Several groups have reported interesting results of chiral spin textures in heterostructures formed with FGT-3 and spin-orbit-coupled materials such as WTe_2 , graphene [3, 4]. Furthermore, the material shows Kondo scattering behavior at low temperatures. Even more interestingly, a direct correlation was found between the ferromagnetism and the effective electron mass, suggesting the system to exhibit the behavior of heavy fermions in this 3d itinerant magnetic system with partially filled d-band [5].

Although the system clearly exhibits ferromagnetic behavior in the entire ordered range [1], some anomalies in the magnetization versus temperature ($M - T$) as well as T -dependent local magnetic imaging of domains using magnetic force microscopy measured on bulk crystals grown by chemical vapor transport (CVT) method lead to the suggestion of coexisting ferromagnetic and complex antiferromagnetic phases in a wide temperature range with an antiferro-

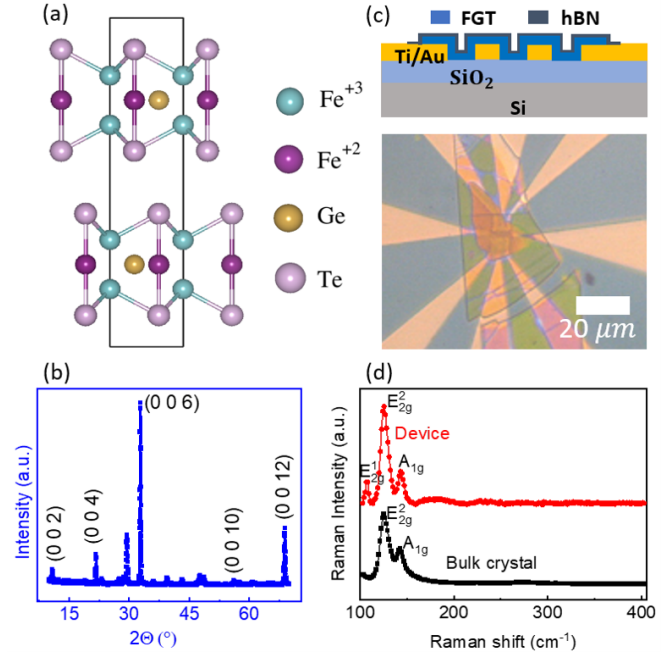


FIG. 1. Crystal structure and device fabrication of FGT-3. (a) The crystal structure of a bilayer FGT-3. Monolayer FGT-3 contains two types of Fe atoms, Fe^{+3} and Fe^{+2} , at different sites. (b) The X-ray diffraction pattern of FGT-3 single crystal. (c) Schematic diagram of the device geometry (top panel). The optical micrograph of fabricated FGT-3/hBN device (bottom panel). (d) Raman spectra of FGT-3 single crystal (black) & the nanoflake of FGT-3 device (red).

magnetic ground state [6]. Later, a kink in the T -dependent Hall response of mechanically exfoliated thin layers of FGT-3 (thickness ≥ 30 nm) was suggested to be a signature of competing ferromagnetism and interlayer antiferromagnetism in the system [7]. The exfoliation was performed in a glove box with a significant oxygen environment of about 20 ppm, and thus, there is an uncertainty of the quality of the devices. These results suggested an interlayer antiferromagnetic cou-

pling between the ferromagnetic Fe-atom planes. However, a few other works suggested the antiferromagnetic phase exhibiting the exchange bias effect is due to the oxidized FGT-3 layer [8]. A recent work based on analysis of ac-susceptibility results suggested 2D spin-glass behavior in the FGT-3 system [9]. Thus, it is clear that inspite of a large number of investigations carried out for this class of systems, a clear understanding of the magnetic ordering of the systems has not been achieved so far. A detailed analysis of magnetization as well as magnetotransport behavior of the same crystals may be helpful to converge the actual physics governing the antiferromagnetic behavior of the system. An understanding of this aspect is critical for the use of the material in any real spintronic devices.

In this work, we have carried out a detailed analysis of the magnetization of bulk crystals and the magneto-transport behavior of thin film of FGT-3 samples exfoliated in a very inert atmosphere. To avoid ambiguity and sample-to-sample variations, the same crystals were used for both investigations. For magneto-transport behavior, primarily the anomalous Hall effect was probed so that a direct correlation between the magnetization and the Hall effect is established. Together with the detailed first-principles calculations, our experimental results provide a clear indication of an intra-layer antiferromagnetic coupling, in addition to a strong interlayer ferromagnetic coupling, which so far has been undetected.

II. EXPERIMENTAL AND COMPUTATIONAL DETAILS

Single crystals of FGT-3 were grown by CVT method and were obtained from commercial sources (viz., HQ graphene). The crystals were characterized by X-ray diffraction and Raman spectroscopy experiments performed at room temperature. Magnetic measurements were carried out using a Magnetic Property Measurement System (make: Quantum Design) under zero field cool (ZFC) and Field cooled cool (FCC) protocols. For the analysis of thermal hysteresis, measurements of magnetization (M) were performed using field cooled warming (FCW) protocol.

For measurements of anomalous Hall effect (AHE), mechanically exfoliated thin layers of FGT-3 devices encapsulated with hexagonal boron nitride (hBN) were used. The same batch of single crystals, as used for the magnetic measurements, was chosen for the transport measurements. The flakes were exfoliated by the conventional scotch tape method on the polydimethylsiloxane (PDMS) and then dry transferred on Hall cross geometry pre-patterned on Si/SiO₂ substrates by optical lithography followed by electron-beam deposition of Ti/Au and lift-off. Further, the transfer process was repeated for hBN without breaking the vacuum to prevent oxidation of the topmost FGT-3 layer. The entire fabrication process was carried out in an inert atmosphere, inside an argon-filled glovebox with O₂ as well as H₂O level of ≤ 0.1 ppm. The bottom contact was chosen so that the entire process of transfer and encapsulation can be carried out without breaking the vacuum. The devices were wire bonded to leadless chip carriers for measurements in a Physical Property Measurement

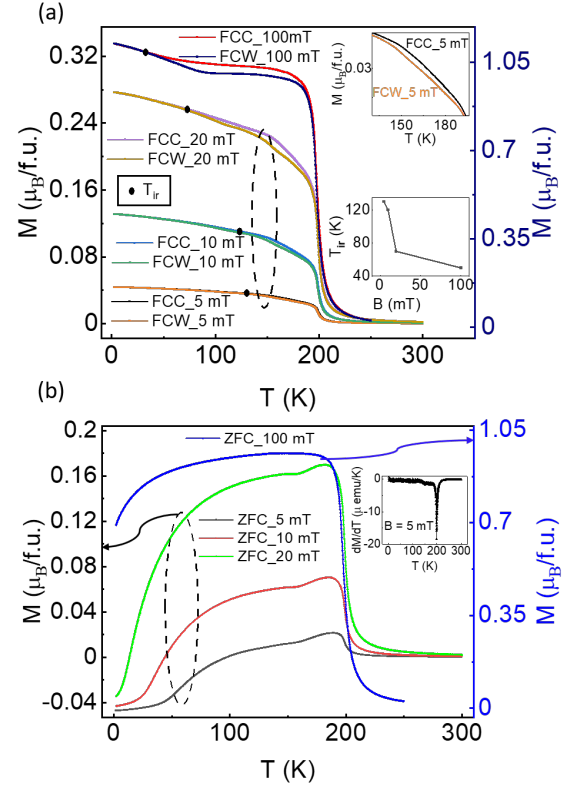


FIG. 2. (a) The magnetization at different applied fields ranging from 5 mT to 100 mT showing the thermo-hysteresis between FCC & FCW curves. The top and bottom right insets indicate the zoomed M - T curve at the field of 5 mT and the irreversibility temperature (T_{ir}) at different applied fields, respectively. (b) ZFC curves at various applied magnetic fields showing a kink near 160 K. Inset shows the derivative of magnetization at 5 mT, indicating the $T_C = 198.6$ K.

System (PPMS) (make: Cryogenics, UK).

To support our experimental results, we performed density functional theory (DFT) based first-principles calculations using the projected augmented wave (PAW) method [10] as implemented in the *Vienna Ab initio Simulation Package* (VASP) [11–13]. The exchange-correlations among electrons were incorporated using the generalized gradient approximation (GGA) based Perdew-Burke-Ernzerhof (PBE) pseudopotential [14]. All calculations employed a plane-wave basis with an energy cutoff of 500 eV. The energy and force convergence criteria were set at 10^{-6} and 10^{-5} eV, respectively, for all self-consistent-field calculations. The conjugate gradient algorithm was employed for structural relaxation, performed on a Γ -centered k -grid of $16 \times 16 \times 4$. To incorporate the effect of strongly correlated 3d-electrons of Fe, on-site Coulomb interaction was included using the rotationally invariant DFT+U approach of Dudarev et al. [15]. Our computed U value, 4.4 eV, is in good agreement with the reported value 4.3 eV and 4.8 eV [16]. However, it is reported that the DFT+U method cannot give an accurate magnetic moment of Fe atoms [16, 17]. It overestimates the magnetic moment by almost $1 \mu_B$. Therefore, for magnetic moment calculation, we

ignore U correction.

III. RESULTS & DISCUSSION

Fe_3GeTe_2 crystallizes in space group of $P6_3/mmc$ has a layered structure with Fe_3Ge layer sandwiched between two Te layers as shown in Fig. 1(a). The Fe_3Ge layer consists of two inequivalent Fe atoms, viz., Fe^{+3} and Fe^{+2} . Each monolayer of FGT-3 is ~ 0.8 nm thick. The unit cell structure consisting of bilayers with van der Waals gap of 0.295 nm between two adjacent layers is shown in Fig. 1(a).

The crystal structure and phase purity of the crystals are confirmed from powder-X-ray diffraction (XRD) measurements performed at room temperature using an X-ray diffractometer (make: Malvern PANalytical; MODEL: Empyrean) with $\text{Cu-K}\alpha$ radiation as source. The XRD pattern shows in the prominent (0,0,2n) peaks where $n = 1, 2, 3, \dots$. A few additional peaks from other different planes from the crystallites in the powder, typical for a powder XRD pattern from, are also observed (Fig. 1(b)) [18]. The XRD pattern confirms the phase purity of the crystals. The Raman spectroscopy result for the single crystal (bulk) FGT-3 is shown in Fig. 1(d). The spectrum shows peaks at 125 cm^{-1} & 143 cm^{-1} corresponding to E_{2g}^2 and A_{1g} modes respectively. A hump-like feature at 103 cm^{-1} is observed, which is suggested to be the position of E_{2g}^1 peak with significantly reduced intensity in bulk crystal [19]. The observed modes are consistent with the reported results, further demonstrating the purity of the crystals.

Fig. 2 shows detailed magnetization data measured under ZFC, FCW, and FCC protocols. T_C , as determined from the derivative of $M - T$ data measured at 5 mT field applied out of plane (easy axis) of the sample, is found to be 198.6 K (see inset of Fig. 2(b)). ZFC and FCW measurements show a bifurcation in the temperature range of 30 K to 130 K depending on the applied field. Such splitting of ZFC and FCW data suggests magnetic irreversibility, typically observed in spin-glass systems. However, this behavior alone is not a direct test of spin-glass behavior and may indicate other complex phenomena (see discussions below). Further, a kink is observed at a temperature close to 160 K- in low-field ZFC curves which vanishes in the higher field data (e.g., 100 mT), see Fig. 2 (b). The kink is further investigated by performing FCC and FCW measurements. A hysteresis is observed in the FCC and FCW data at around the same temperature where a kink is observed in ZFC data (see Fig. 2(b)). This indicates that the magnetic moments do not follow the same orientation dynamics with temperature during cooling and warming cycles. Interestingly, the position of the hysteresis monotonically shifts to lower T as the field is increased from 5 mT to 100 mT. This is clearly observed from the irreversibility temperature (T_{ir}), marked by closed circles in the corresponding $M - T$ plots. T_{ir} refers to the temperature at which the bifurcation between FCC and FCW starts while warming up. The lower inset in Fig. 2a shows the plot of T_{ir} vs T . The shift in T_{ir} with T is tabulated in table I. Moreover, at low temperature, the ZFC curve measured at a small OOP field of up to 20 mT reduces to a negligible value of magnetization. The behavior of thermo-

hysteresis in magnetization suggests the presence of different magnetic interactions, such as due to the coexistence of magnetic phases, in the system [20].

Earlier, Yi, *et al.* had reported observation of such thermohysteresis and kinks in corresponding $M - T$ results obtained from CVT-grown FGT crystals. Thus, our results of the magnetization of bulk crystals are very consistent with those reported for the CVT-grown sample. The unusual behavior of magnetization under different conditions was suggested by Yi, *et al.* to be due to the presence of competing ferro-(FM) and antiferro-magnetically (AFM) ordered Fe moments in the system [6]. Based on the magnetization and ac-susceptibility measurements, an AFM ground state as well as a coexisting AFM and FM states in the temperature range of $\sim 150 - 200$ K was suggested to be responsible for the thermohysteresis behavior. Additionally, recently Chyczewski *et al.* have reported an unusual behavior in magnetotransport characteristics of exfoliated Fe-doped FGT crystals [7]. Peaks in the $dR_{xy}/d(\mu_0 H)$ as well as MR vs T as observed at $T \sim 120$ K were considered as the signature for an AFM phase in the crystal. Both of these works suggested an interlayer AFM coupling between Fe ions, coexisting with in-plane ferromagnetic interactions between other Fe ions, for this system. We note here that although an AFM spin ordering was suggested as the origin of an unusual peak observed in the magnetotransport data, no direct evidence of this has been found in the transport data so far. Moreover, the literature, which is very limited on this problem, shows contradictory suggestions on the AFM interactions in the system [21]. Thus, it is clear that a detailed investigation of this aspect is absent in the literature.

The analysis of magnetization switching behavior of individual layers of FGT-3 crystals may provide important insight into this problem. Fig. 3(a) shows the magnetization behavior of few-layered flakes along with that of a bulk FGT-3 crystal measured by SQUID magnetometry in an MPMS. Contrary to the continuous change in magnetization observed for bulk crystals, interestingly, a sharp jump, along with a few irregularities at a few discrete field values, is observed for the flakes. Such sharp steps in magnetization in a ferromagnet are typically observed as Barkhausen jumps resulting from pinning and depinning of domain walls. We find that these steps always occur at the same external field values, thereby representing the magnetization changes due to intrinsic switching of magnetic moments, most likely in specific layers of FGT-3. Thus, they are expected to occur at certain specific field values. Based on our observation of the magnetization of the bulk crystals, it appears that such characteristic switching behavior may be clearly observed in thinner samples. Thus, to further investigate the detailed behavior of the switching in thinner samples, we attempted to perform anomalous Hall effect (AHE) measurements on a few-layer flakes of the FGT-3 crystals. To avoid any oxidation of surfaces and carry out the magneto-transport experiments on pristine samples, the entire process of fabrication of the encapsulated sample of ~ 20 layers was carried out in a glove box as mentioned above. The level of O_2 and humidity of ≤ 0.1 ppm is critical to the results obtained as discussed below.

The thin flake, as shown in Fig. 1(d), is characterized by

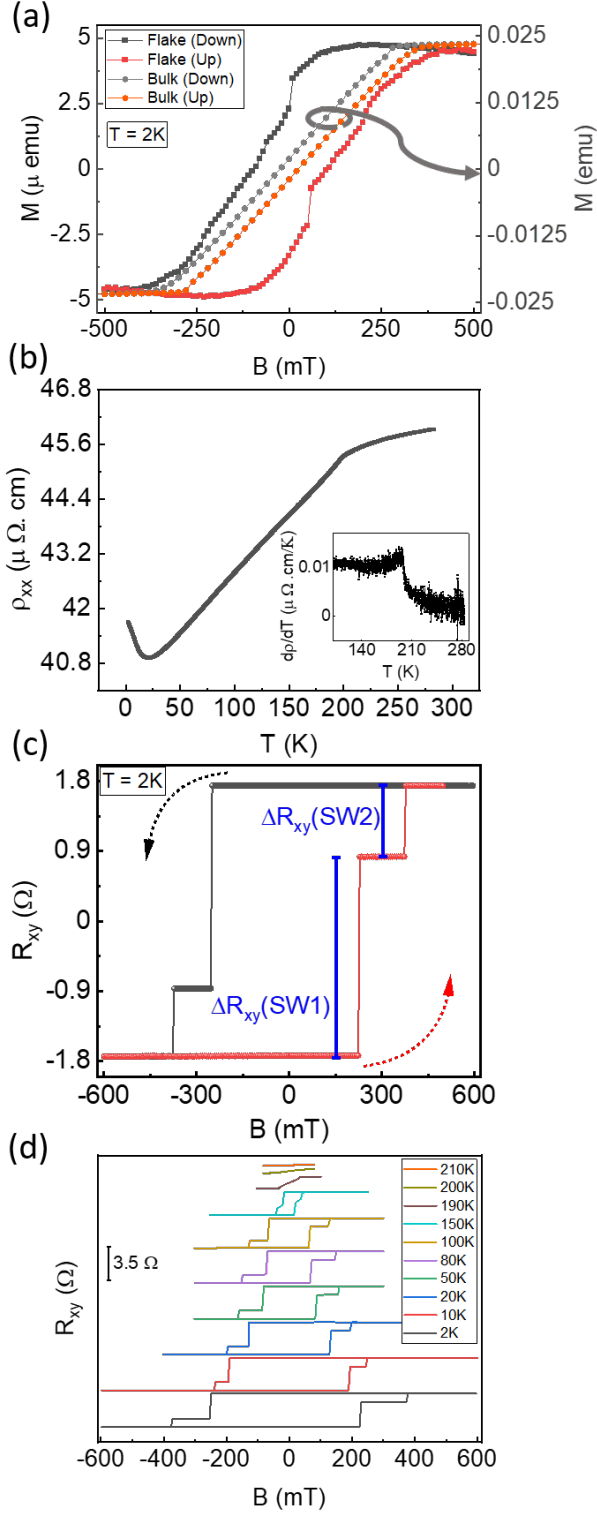


FIG. 3. The magneto-transport behavior of FGT-3/hBN device. (a) M - H of few-layer flakes and bulk single crystal of FGT-3 at $T = 2\text{K}$. (b) The temperature-dependent resistivity of a few-layer (~ 20 layers) FGT-3 device. (Inset) The derivative of the resistivity curve showing the T_C of 196 K. (c) Anomalous Hall effect of a ~ 20 layers FGT-3 device at $T = 2\text{K}$. (d) The temperature evolution of the anomalous Hall behavior of the FGT-3 device.

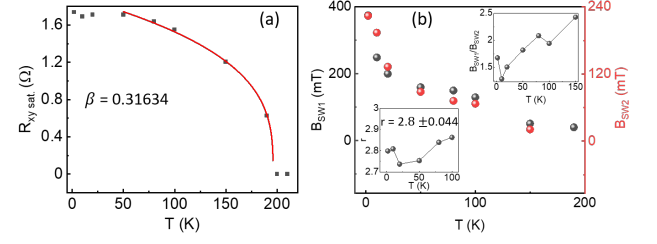


FIG. 4. (a) Temperature dependence of anomalous Hall resistance (R_{xy}) at saturation field. The red curve is the critical exponent power law equation fit, where β is the critical exponent. (b) T -dependence of the switching fields at first switching (B_{SW1}) and second switching (B_{SW2}). (Inset) T -dependence of the ratio $B_{\text{SW1}}/B_{\text{SW2}}$ (top) and $r = \Delta R_{xy}(\text{SW1})/\Delta R_{xy}(\text{SW2})$ (bottom). Here $\Delta R_{xy}(\text{SW1},2)$ represent the change in R_{xy} at SW1 and SW2, respectively.

the Raman spectroscopy measurements. The Raman spectrum exhibits two clear peaks as observed for the bulk sample. An additional peak at 108cm^{-1} is also observed for the flake. The intensity of Raman mode near 110cm^{-1} becomes more prominent at thin layers, consistent with a theoretical study by X. Kong, *et al.* [19]. Thus, we confirm the pristine crystalline quality of the flake after device fabrication. Fig. 3(b) shows the temperature-dependent resistivity ($\rho - T$) curve measured for the encapsulated FGT-3 flake. The change in slope, determined by a derivative of $\rho - T$ curve (see inset), suggests T_C of 196 K, slightly lower than that of the bulk sample, determined from the magnetization measurements. An upturn in resistivity is observed below $T \sim 20\text{K}$, which is consistent with the data reported in literature [5, 22]. As discussed above, FGT-3 shows itinerant ferromagnetic behavior due to Fe^{+3} ions and localized behavior due to Fe^{+2} ions [2]. The presence of localized magnetic moments effectively acts as internal magnetic impurities, whose interaction with conduction electrons induces a characteristic Kondo upturn in resistivity at low temperatures. The AHE measured at $T = 2\text{K}$ for the device is shown in Fig. 3(c). The AHE exhibits two sharp jumps in R_{xy} at external field values of 224 mT (switching 1 - SW1) and 375 mT (switching 2 - SW2), respectively while up sweep. Considering that the AHE is due to the magnetization of the sample, these jumps suggest two-level switching of magnetization in response to the applied field. Similar to our observation of field-dependent non-stochastic behavior of the jumps observed for $M - H$ curves for flakes, these jumps in R_{xy} are also found to occur each time at the same fields during multiple field sweeps carried out to verify the (non-)stochasticity of the jumps. Moreover, the change in Hall resistance ΔR_{xy} during the two switching processes exhibits a characteristic behavior, viz., $\Delta R_{xy}(\text{SW2}) > \Delta R_{xy}(\text{SW1})$. This characteristic behavior is consistently observed in the temperature dependence of R_{xy} vs B . As shown in Fig. 3(d), the two sharp switchings in the hysteresis loop of R_{xy} vs B persist till the T_C . However, additional features such as linear variation of R_{xy} vs B after the 1st switching and a non-linear change before saturation emerge at temperatures between $T \sim 100 - 150\text{K}$.

The ZFC M-T curves (Fig. 2 (b)) show the magnetic moment has a sudden increase near $T \sim 160$ K which is due to the dominance of FM coupling in the system as the AFM coupling vanishes at $T \sim 160$ K due to the decrease in the magnetic anisotropy at higher temperatures. These observations suggest that the jumps in R_{xy} vs B are likely to be due to an intrinsic magnetization switching process of different inequivalent Fe atoms in the individual layers. A weak non-linear response of R_{xy} is observed till $T \sim 200$ K which becomes perfectly linear at $T = 210$ K suggesting that the T_C as observed from the slope change of R_{xx} may not be the true thermodynamic Curie temperature as indirectly determined from AHE measurements. Such a discrepancy of T_C from electrical transport and magnetization measurements is often observed as the resistivity measurements depend on the short-range ordering of magnetic moments, which may often persist beyond the true thermodynamic value of T_C , which represents the onset of long-range order in the system. In such cases, the anomaly in resistivity appears at a higher temperature than the thermodynamic value of T_C . However, in our case, the observation of T_C determined from R_{xy} vs T is lower than that determined from the response of AHE. This suggests that T_C determined from resistivity anomalies may differ from the actual T_C reported for thin flakes of such van der Waals materials, where performing magnetization measurements is challenging due to the small volume of the thin flake samples. For our FGT-3 samples, the difference (discrepancy!) in T_C values is of ~ 5 K.

From the T -dependent data, we note further three important observations - the T -dependence of R_{xy} at saturation shows $(T_C - T)^\beta$ type behavior with critical exponent $\beta = 0.316$, See Fig. 4(a). The value of $\beta = 0.316$ suggests a 3D Ising-type interaction in the system. Secondly, we further observe that the external fields (B_{SW1} , B_{SW2}) for the switchings SW1 and SW2, respectively, systematically reduce as a function of T . As fluctuations of magnetization (M) increase with T , the uniaxial anisotropy energy density (K) reduces with an increase in T . Thus, a monotonous behavior of B_{SW1} and B_{SW2} , as shown in Fig. 4(b), are observed as a function of T . Third, the ratio B_{SW1}/B_{SW2} shows a linearly increasing behavior as a function of T , clearly suggesting that the two sharp switchings are due to the magnetization reversal of Fe magnetic moments with different T -dependent anisotropy behavior. Interestingly, we also find that although ΔR_{xy} at each switching varies as a function of T , the ratio $\Delta R_{xy(SW1)}/\Delta R_{xy(SW2)}$ remains nearly constant at ~ 2.8 with slight reduction in the T range of 20 - 40 K, see left-inset of Fig. 4(b). Here $\Delta R_{xy(SW1,2)}$ represent the change in R_{xy} at SW1 and SW2, respectively.

We note that sharp single switching for thin FGT-3 flakes was reported earlier for very high-quality devices fabricated in a controlled atmosphere; however, for devices with top-contact [1, 4, 23]. The analysis, as discussed above, suggests that the sharp two switchings for the FGT-3 device in this case may be related to coherent magnetization reversal of two different sets of Fe moments in the unit cells. In order to achieve an in-depth understanding of this double switching behavior, we carry out a theoretical analysis of magnetization using den-

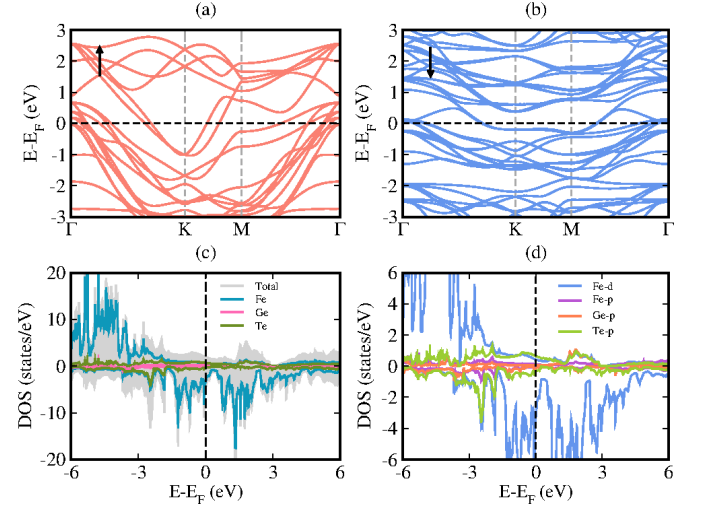


FIG. 5. The spin polarized electronic band structure of Bulk FGT, (a) & (b) spin-up and spin-down channels, respectively. Panels (c) & (d) The atom-projected and orbital-projected density of states, respectively. The Fermi level is set to zero.

TABLE I. The shift in the thermo-hysteresis between FCC & FCW M - T curves towards higher T as the field reduces from 100 mT to 5 mT. Here the irreversibility temperature (T_{ir}) refers the temperature where the bifurcation between FCC and FCW starts.

Irreversibility Temperature T_{ir} (K)	B (mT)
130	5
120	10
70	20
30	100

sity functional theory based first-principles calculations.

From our calculations, we first checked the consistency of our theoretical analysis with the corresponding reported values in literature. We begin with the experimental lattice parameters to achieve the ground state of the system. Our calculated lattice constants ($a = b = 3.990$ Å, $c = 16.329$ Å) are consistent with our experimental results ($a = b = 3.99$ Å, $c = 16.35$ Å) as well as previously reported values ($a = b = 3.991$ Å, $c = 16.33$ Å) [24]. The optimized structure is further used to examine the electronic structure of the material. We have calculated spin-polarized band structure and density of states (DOS), as shown in Fig. 5. As discernible from panels (a) and (b) of Fig. 5, FGT-3 exhibits a metallic nature. This is consistent with the metallic nature observed for FGT-3 [25, 26]. In panels (c) and (d) of Fig. 5, we show the total DOS, atom-projected DOS and orbital-projected DOS, respectively. Consistent with the bands, the DOS also show a metallic behavior, however, with an asymmetry in the states associated with spin-up and spin-down channels. The lower valence bands in the energy range from -6 to -3 eV mainly originate from the hybridization of Fe- d , Ge- p and Te- p orbitals. The upper valence and lower conduction bands (-2 to 1 eV) are mainly dominated by Fe- d orbitals with some minor contributions of

TABLE II. Computed ground state magnetic properties for bulk and monolayer FGT. The bulk results include the total energy (in eV/f.u.) of the FM, AFM configurations and their difference ($\Delta E = E_{\text{FM}} - E_{\text{AFM}}$) (in meV), magnetic anisotropy energy ΔE_{MAE} (in meV), magnetic moments of Fe, Ge and Te atoms ($\mu^{\text{Fe}^{+3}}$, $\mu^{\text{Fe}^{+2}}$, μ^{Ge} , μ^{Te}) (in μ_B/atom), total magnetic moment (μ^{Total}) (in $\mu_B/\text{f.u.}$), and interlayer exchange coupling constant J_z (in meV). The monolayer results include the total energies for FM and various AFM configurations (E_{FM} , E_{AFM1} , E_{AFM2} , E_{AFM3}) (in eV/f.u.), and the exchange coupling constants J_1 and J_2 (in meV). Reported values are shown for comparison.

	Our result	Reported result
FGT Bulk		
ΔE_{MAE}	5.63	3.37 [25]
E_{FM}	-27.1736	-
E_{AFM}	-27.1660	-
ΔE	-15.11	-
$\mu^{\text{Fe}^{+3}}$	2.35	2.41 [25]
$\mu^{\text{Fe}^{+2}}$	1.43	1.53 [25]
μ^{Ge}	-0.09	-0.10 [25]
μ^{Te}	-0.03	-0.04 [25]
μ^{Total}	5.97	6.29 [25]
J_z	3.7	
FGT monolayer		
E_{FM}	-26.7691	
E_{AFM1}	-26.9105	
E_{AFM2}	-26.9226	
E_{AFM3}	-26.9514	
J_1	-0.47	-0.44 [27]
J_2	1.24	3.27 [27]
J_2/J_1	2.63	

Te p-orbitals around the Fermi level. It is clear that the metallic character of FGT mainly arises from the *d*-orbital of Fe.

To investigate, the magnetic properties of FGT-3 using first-principles calculations, we first check the consistency of our results of computations with the values reported in literature. We first examined the energetics for both ferromagnetic (FM) and antiferromagnetic (AFM) configurations for the system. The results of our calculations for total energies for FM and AFM configurations are given in Table II. The results show the FM ground state for bulk FGT-3, which has 7.6 meV lower energy than for the AFM state. This is consistent with our experiments and other reported literature [1, 28]. We have also computed the magnetic moment of individual elements, as given in Table II. Our calculated magnetic moments of Fe^{+3} & Fe^{+2} are 2.35 and 1.43 μ_B per atom, respectively, which are in good agreement with the previously reported values [25]. The dominant contribution to magnetism is clearly from the unpaired *d*-electrons of Fe ions.

Magnetocrystalline anisotropy energy (MAE), defined as $E_{\text{MAE}} = E_{\text{IP}} - E_{\text{OOP}}$, where E_{IP} and E_{OOP} is total energy for in-plane and out-of-plane configurations, respectively, was calculated next. A positive magnetic anisotropy energy of 5.63 meV was found, indicating an out-of-plane spin anisotropy for FGT-3, which is also consistent with our experimental findings and other reported literature [25].

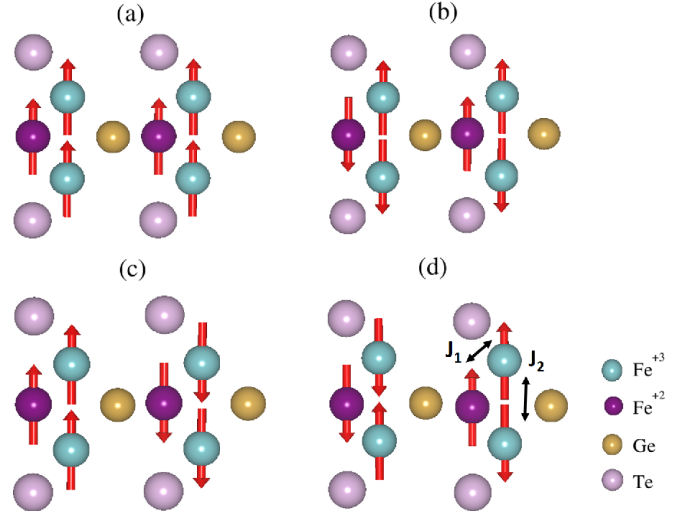


FIG. 6. The schematic of (a) FM, (b) AFM-1, (c) AFM-2, and (d) AFM-3 magnetic configurations of monolayer FGT and J_1 & J_2 are schematic representations of the exchange interaction between Fe atoms of the FGT-3 monolayer.

In order to investigate the origin of the sharp double switchings in our AHE data, we next examined the interlayer and intralayer exchange coupling constants in FGT-3. Using the Heisenberg model Hamiltonian

$$H = E_0 - \sum_{i>j} J_{ij} (\hat{e}_i \cdot \hat{e}_j)$$

we find interlayer exchange coupling constant (J_z) = 3.7 meV. Here, E_0 is the magnetic configuration independent part of the total energy, J_{ij} is the exchange coupling parameter, and \hat{e}_i is the unit vector representing the direction of the magnetic moment on site *i*. The positive J_z signifies an FM interaction between adjacent layers in FGT-3. We next focus on the details of intralayer exchange interactions. We examine the magnetic ground state of monolayer FGT-3 using a 2*1*1 supercell. By fixing a prior spin orientations of Fe^{+3} and Fe^{+2} ions in a monolayer, we consider four different possible magnetic configurations as shown in Fig. 6(a)-(d). Depending on the assumed spin orientation of Fe atoms, the four magnetic configurations, one FM and the other three AFM, viz., AFM1, AFM2, and AFM3, were considered. We determine the energetics for each of these configurations for monolayer FGT-3, which we list in Table II. From our detailed calculations, we find the ground state of monolayer FGT-3 is of configuration AFM3 with energy difference (ΔE) of 182.3 μeV , whereas the ΔE for AFM1 configurations is $\sim 141 \mu\text{eV}$ with respect to the FM configuration. Because of such a small energy difference between an FM and AFM configurations, very small changes in stoichiometry or positional configuration of Fe^{+3} and Fe^{+2} ions may lead to stabilization of FM ground state in real crystals. As the unit cell of FGT-3 contains Fe^{+2} as well as Fe^{+3} ions, we further calculate the exchange coupling constants J_1 and J_2 between the Fe^{+3} - Fe^{+3} and Fe^{+2} - Fe^{+3} ions, respectively for the ground state configuration, see Fig. 6 (d). We find $J_1 = 1.24$ meV and $J_2 = -0.47$ meV. Thus, these

calculations suggest an AFM interaction between Fe^{+3} - Fe^{+3} spins whereas a FM interaction is found between Fe^{+3} and Fe^{+2} spins.

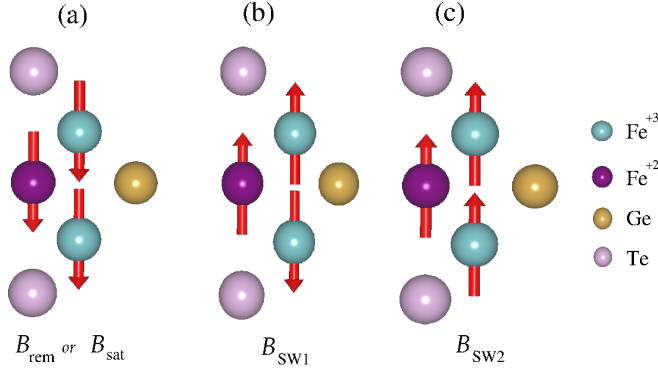


FIG. 7. The schematic of magnetic moments of Fe^{+3} and Fe^{+2} at remanence (B_{rem}) or saturation (B_{sat}) and two different switching fields (B_{SW1}) & (B_{SW2}).

In order to validate the two types of exchange interactions among the different Fe-ions, we next analyze the changes in the magnetization (ΔM_1 and ΔM_2) during the switchings at external fields B_{SW1} and B_{SW2} , respectively. Fig. 7 shows the behavior of Fe^{+3} and Fe^{+2} moments at remanence and two different switching fields. The remanence and saturation states are the same. While upsweeping the field from remanent state, as the field is increased in the opposite direction, all ferromagnetically coupled Fe^{+3} and Fe^{+2} moments switch at B_{SW1} , thereby inducing a sharp step-like change in magnetization ΔM_1 and thereby the corresponding AHE $\Delta R_{xy}(\text{SW1})$. The AFM coupled Fe^{+3} spins switch at higher field (B_{SW2}). The change in magnetization ΔM_2 due to this switching is less than for the 1st switching, as in this case, only those spins that are oppositely directed switch. The corresponding change in $\Delta R_{xy}(\text{SW2})$ as observed in our experiment is about $\frac{1}{3}$ rd of $\Delta R_{xy}(\text{SW1})$. Thus, we find a qualitative agreement between our observed experimental results of $\Delta R_{xy}(\text{SW1})$ and $\Delta R_{xy}(\text{SW2})$ and theoretical calculations. Furthermore, we also observe that the ratio $J_1/J_2 \approx 2.63$, which is nearly of similar value as that for the ratio $\Delta R_{xy}(\text{SW1})/\Delta R_{xy}(\text{SW2})$ obtained from our experimental measurements. As discussed above, $\Delta R_{xy}(\text{SW1})$ and $\Delta R_{xy}(\text{SW2})$ correspond to switchings of ferromagneti-

cally ($\sim J_1$) and antiferromagnetically aligned spins ($\sim J_2$), respectively.

Finally, we note from the temperature dependent R_{xy} vs B data that the 2nd switching vanishes between $T \sim 150$ K and 190 K which is again consistent with the observation of a kink-like feature at $T \sim 160$ K observed in the $M-T$ (ZFC) data as shown in Fig. 2(b). As discussed above, the kink-like feature is most likely due to the AFM transition (T_N) at ~ 160 K. The observed $T_N < T_C$ is also consistent with the calculated values of corresponding exchange coupling values, viz., $J_1 < J_2$.

Thus, from all our bulk magnetization and AHE results as well as first-principles calculations, we find a consistent and clear signature of an intra-layer antiferromagnetic coupling between Fe^{+3} and Fe^{+3} moments in FGT-3 crystals. Our results show that detailed analysis of bulk magnetization and magnetotransport behavior of high-quality samples fabricated in a very clean environment is important to extract intrinsic behavior of magnetization of such van der Waals magnets. Our work may pave the way to exploring new magnetic phases and designing future spintronic devices.

ACKNOWLEDGMENTS

PD gratefully acknowledges the funding support from the Science & Engineering Research Board (SERB) of Govt. of India (grant no. SPR/2021/000762). BKM acknowledges the funding support from SERB, DST (CRG/2022/000178). NY is thankful to the Council of Scientific & Industrial Research (CSIR) for financial support. Shivani acknowledges the fellowship support from UGC (BININ01949131), Govt. of India. Sandeep is thankful to Ministry of Education (MoE) for the financial support. NY, Sandeep & PD acknowledge the Dept of Physics, Central Research Facility (CRF) and Nano Research Facility (NRF), Indian Institute of Technology (IIT) Delhi, for availing of various experimental facilities. Shivani & BKM are thankful to High Performance Computing cluster Tejas at the Indian Institute of Technology Delhi and PARAM Rudra, a national supercomputing facility at Inter-University Accelerator Centre (IUAC), New Delhi.

DATA AVAILABILITY STATEMENT

The data supporting this study's findings are available from the corresponding author upon reasonable request.

- [1] Y. Deng, Y. Yu, Y. Song, J. Zhang, N. Z. Wang, Z. Sun, Y. Yi, Y. Z. Wu, S. Wu, J. Zhu, *et al.*, Gate-tunable room-temperature ferromagnetism in two-dimensional fe_3gete_2 , *Nature* **563**, 94 (2018).
- [2] P. R. Sharma, T. W. Kim, and H. Noh, Non-monotonic temperature dependence of anomalous hall effect in a 2D van der waals ferromagnetic material fe_3gete_2 , *Materials Chemistry and Physics* **302**, 127738 (2023).

- [3] Y. Wu, S. Zhang, J. Zhang, W. Wang, Y. L. Zhu, J. Hu, G. Yin, K. Wong, C. Fang, C. Wan, *et al.*, Néel-type skyrmion in $\text{wte}_2/\text{fe}_3\text{gete}_2$ van der waals heterostructure, *Nature communications* **11**, 3860 (2020).
- [4] P. K. Srivastava, Y. Hassan, S. Lee, M. Joe, M. S. Abbas, H. Ahn, A. Tiwari, S. Ghosh, W. J. Yoo, B. Singh, *et al.*, Unusual dzyaloshinskii-moriya interaction in $\text{graphene}/\text{fe}_3\text{gete}_2$ van der waals heterostructure, *Small* **20**, 2402604 (2024).

- [5] Y. Zhang, H. Lu, X. Zhu, S. Tan, W. Feng, Q. Liu, W. Zhang, Q. Chen, Y. Liu, X. Luo, *et al.*, Emergence of kondo lattice behavior in a van der Waals itinerant ferromagnet, *Fe₃GeTe₂*, *Science advances* **4**, eaao6791 (2018).
- [6] J. Yi, H. Zhuang, Q. Zou, Z. Wu, G. Cao, S. Tang, S. Calder, P. Kent, D. Mandrus, and Z. Gai, Competing antiferromagnetism in a quasi-2D itinerant ferromagnet: *Fe₃GeTe₂*, *2D Materials* **4**, 011005 (2016).
- [7] S. T. Chyczewski, J. Shi, H. Lee, P. F. Furlanetto, K. Xu, A. M. van der Zande, and W. Zhu, Probing antiferromagnetism in exfoliated *Fe₃GeTe₂* using magneto-transport measurements, *Nanoscale* **15**, 14061 (2023).
- [8] D. Kim, S. Park, J. Lee, J. Yoon, S. Joo, T. Kim, K.-j. Min, S.-Y. Park, C. Kim, K.-W. Moon, *et al.*, Antiferromagnetic coupling of van der Waals ferromagnetic *Fe₃GeTe₂*, *Nanotechnology* **30**, 245701 (2019).
- [9] B. Pal, A. K. Gopi, Y. Guan, A. Chakraborty, K. Tiwari, A. Mathew, A. K. Srivastava, W. Zhang, B. K. Hazra, H. Meyerheim, *et al.*, Realization of a spin glass in a two-dimensional van der Waals material, *arXiv preprint arXiv:2403.02088* (2024).
- [10] P. E. Blöchl, Projector augmented-wave method, *Physical Review B* **50**, 17953 (1994).
- [11] G. Kresse and D. Joubert, From ultrasoft pseudopotentials to the projector augmented-wave method, *Physical Review B* **59**, 1758 (1999).
- [12] G. Kresse and J. Hafner, Ab initio molecular-dynamics simulation of the liquid-metal–amorphous-semiconductor transition in germanium, *Physical Review B* **49**, 14251 (1994).
- [13] G. Kresse and J. Furthmüller, Efficient iterative schemes for ab initio total-energy calculations using a plane-wave basis set, *Physical Review B* **54**, 11169 (1996).
- [14] J. P. Perdew, K. Burke, and M. Ernzerhof, Generalized gradient approximation made simple, *Physical Review Letters* **77**, 3865 (1996).
- [15] M. Cococcioni and S. De Gironcoli, Linear response approach to the calculation of the effective interaction parameters in the *Lda+u* method, *Physical Review B—Condensed Matter and Materials Physics* **71**, 035105 (2005).
- [16] S. Ghosh, S. Ershadrad, V. Borisov, and B. Sanyal, Unraveling effects of electron correlation in two-dimensional *Fe_nGeTe₂* ($n = 3, 4, 5$) by dynamical mean field theory, *npj Computational Materials* **9**, 86 (2023).
- [17] H. L. Zhuang, P. Kent, and R. G. Hennig, Strong anisotropy and magnetostriction in the two-dimensional stoner ferromagnet *Fe₃GeTe₂*, *Physical Review B* **93**, 134407 (2016).
- [18] S. Bera, S. K. Pradhan, R. Pal, B. Pal, A. Bera, S. Kalimuddin, M. Das, D. S. Roy, H. Afzal, A. N. Pal, *et al.*, Enhanced coercivity and emergent spin-cluster-glass state in 2D ferromagnetic material, *Fe₃GeTe₂*, *Journal of Magnetism and Magnetic Materials* **583**, 171052 (2023).
- [19] X. Kong, T. Berlijn, and L. Liang, Thickness and spin dependence of Raman modes in magnetic layered *Fe₃GeTe₂*, *Advanced Electronic Materials* **7**, 2001159 (2021).
- [20] S. Pal, K. Kumar, and A. Banerjee, Phase coexistence and nonequilibrium dynamics under simultaneously applied magnetic field and pressure: Possible role of the interface, *Physical Review B* **108**, 214409 (2023).
- [21] J. Ke, M. Yang, W. Xia, H. Zhu, C. Liu, R. Chen, C. Dong, W. Liu, M. Shi, Y. Guo, *et al.*, Magnetic and magneto-transport studies of two-dimensional ferromagnetic compound *Fe₃GeTe₂*, *Journal of Physics: Condensed Matter* **32**, 405805 (2020).
- [22] Y. Huang, X. Yao, F. Qi, W. Shen, and G. Cao, Anomalous resistivity upturn in the van der Waals ferromagnet *Fe₅GeTe₂*, *Applied Physics Letters* **121** (2022).
- [23] Z. Fei, B. Huang, P. Malinowski, W. Wang, T. Song, J. Sanchez, W. Yao, D. Xiao, X. Zhu, A. F. May, *et al.*, Two-dimensional itinerant ferromagnetism in atomically thin *Fe₃GeTe₂*, *Nature materials* **17**, 778 (2018).
- [24] H.-J. Deiseroth, K. Aleksandrov, C. Reiner, L. Kienle, and R. K. Kremer, *Fe₃GeTe₂* and *Ni₃GeTe₂*—two new layered transition-metal compounds: crystal structures, hrtem investigations, and magnetic and electrical properties (2006).
- [25] M.-C. Jiang and G.-Y. Guo, Large magneto-optical effect and magnetic anisotropy energy in two-dimensional metallic ferromagnet *Fe₃GeTe₂*, *Physical Review B* **105**, 014437 (2022).
- [26] T. J. Kim, S. Ryee, and M. J. Han, *Fe₃GeTe₂*: a site-differentiated hund metal, *npj Computational Materials* **8**, 245 (2022).
- [27] Q. Liu, J. Xing, Z. Jiang, Y. Guo, X. Jiang, Y. Qi, and J. Zhao, Layer-dependent magnetic phase diagram in *Fe_nGeTe₂* ($3 \leq n \leq 7$) ultrathin films, *Communications Physics* **5**, 140 (2022).
- [28] X. Kong, G. D. Nguyen, J. Lee, C. Lee, S. Calder, A. F. May, Z. Gai, A.-P. Li, L. Liang, and T. Berlijn, Interlayer magnetism in *Fe₃-xGeTe₂*, *arXiv preprint arXiv:2006.01094* (2020).
- [29] N. D. Mermin and H. Wagner, Absence of ferromagnetism or antiferromagnetism in one-or two-dimensional isotropic Heisenberg models, *Physical Review Letters* **17**, 1133 (1966).
- [30] C. Gong, L. Li, Z. Li, H. Ji, A. Stern, Y. Xia, T. Cao, W. Bao, C. Wang, Y. Wang, *et al.*, Discovery of intrinsic ferromagnetism in two-dimensional van der Waals crystals, *Nature* **546**, 265 (2017).
- [31] S. W. Jang, H. Yoon, M. Y. Jeong, S. Ryee, H.-S. Kim, and M. J. Han, Origin of ferromagnetism and the effect of doping on *Fe₃GeTe₂*, *Nanoscale* **12**, 13501 (2020).
- [32] R. Roemer, C. Liu, and K. Zou, Robust ferromagnetism in wafer-scale monolayer and multilayer *Fe₃GeTe₂*, *npj 2D Materials and Applications* **4**, 33 (2020).
- [33] Z. Fei, B. Huang, P. Malinowski, W. Wang, T. Song, J. Sanchez, W. Yao, D. Xiao, X. Zhu, A. F. May, *et al.*, Two-dimensional itinerant ferromagnetism in atomically thin *Fe₃GeTe₂*, *Nature materials* **17**, 778 (2018).
- [34] C. Tan, J. Lee, S.-G. Jung, T. Park, S. Albarakati, J. Partridge, M. R. Field, D. G. McCulloch, L. Wang, and C. Lee, Hard magnetic properties in nanoflake van der Waals *Fe₃GeTe₂*, *Nature communications* **9**, 1554 (2018).
- [35] P. Saha, M. Singh, V. Nagpal, P. Das, and S. Patnaik, Scaling analysis of anomalous Hall resistivity and magnetoresistance in the quasi-two-dimensional ferromagnet *Fe₃GeTe₂*, *Physical Review B* **107**, 035115 (2023).
- [36] A. Chakraborty, A. K. Srivastava, A. K. Sharma, A. K. Gopi, K. Mohseni, A. Ernst, H. Deniz, B. K. Hazra, S. Das, P. Sessi, *et al.*, Magnetic skyrmions in a thickness tunable 2D ferromagnet from a defect driven Dzyaloshinskii–Moriya interaction, *Advanced Materials* **34**, 2108637 (2022).
- [37] F. M. Oliveira, N. Antonatos, V. Mazánek, D. Sedmidubský, Z. Sofer, and R. Gusmão, Exfoliated *Fe₃GeTe₂* and *Ni₃GeTe₂* materials as water splitting electrocatalysts, *FlatChem* **32**, 100334 (2022).
- [38] Q. C. Point, High pressure-driven magnetic disorder and structural transformation in Fe, *Adv. Sci.*, 2206842 (2023).
- [39] A. F. May, S. Calder, C. Cantoni, H. Cao, and M. A. McGuire, Magnetic structure and phase stability of the van der Waals bonded ferromagnet *Fe_{3-x}GeTe₂*, *Physical Review B* **93**, 014411 (2016).
- [40] H. K. Gweon, S. Y. Lee, H. Y. Kwon, J. Jeong, H. J. Chang, K.-W. Kim, Z. Q. Qiu, H. Ryu, C. Jang, and J. W. Choi, Exchange bias in weakly interlayer-coupled van der Waals magnet

- Fe₃GeTe₂, Nano letters **21**, 1672 (2021).
- [41] L. Zhang, X. Huang, H. Dai, M. Wang, H. Cheng, L. Tong, Z. Li, X. Han, X. Wang, L. Ye, *et al.*, Proximity-coupling-induced significant enhancement of coercive field and Curie temperature in 2D van der Waals heterostructures, *Advanced Materials* **32**, 2002032 (2020).
 - [42] T. Li, S. Jiang, N. Sivasdas, Z. Wang, Y. Xu, D. Weber, J. E. Goldberger, K. Watanabe, T. Taniguchi, C. J. Fennie, *et al.*, Pressure-controlled interlayer magnetism in atomically thin CrI₃, *Nature materials* **18**, 1303 (2019).
 - [43] X. Zeng, G. Ye, S. Huang, L. Zhang, H. Xu, Y. Liu, H. Kuang, B. Ma, J. Luo, X. Lu, *et al.*, Magnetoresistance studies of two-dimensional Fe₃GeTe₂ nano-flake, *Journal of Physics: Condensed Matter* **34**, 345701 (2022).
 - [44] X. Bai, F. Lechermann, Y. Liu, Y. Cheng, A. I. Kolesnikov, F. Ye, T. J. Williams, S. Chi, T. Hong, G. E. Granroth, *et al.*, Antiferromagnetic fluctuations and orbital-selective mott transition in the van der Waals ferromagnet Fe_{3-x}GeTe₂, *Physical Review B* **106**, L180409 (2022).
 - [45] N. Nagaosa, J. Sinova, S. Onoda, A. H. MacDonald, and N. P. Ong, Anomalous Hall effect, *Reviews of modern physics* **82**, 1539 (2010).
 - [46] G. Zheng, W.-Q. Xie, S. Albarakati, M. Algarni, C. Tan, Y. Wang, J. Peng, J. Partridge, L. Farrar, J. Yi, *et al.*, Gate-tuned interlayer coupling in van der Waals ferromagnet Fe₃GeTe₂ nanoflakes, *Physical Review Letters* **125**, 047202 (2020).
 - [47] G. Ma, R. Du, F. Lian, S. Bao, Z. Guo, X. Cai, J. Xiao, Y. Han, D. Zhang, S. Jiang, *et al.*, Tailoring coercive fields and the Curie temperature via proximity coupling in WSe₂/Fe₃GeTe₂ van der Waals heterostructures, *2D Materials* (2024).
 - [48] Z. Tu, T. Zhou, T. Ersevı, H. S. Arachchige, A. T. Hanbicki, A. L. Friedman, D. Mandrus, M. Ouyang, I. Žutić, and C. Gong, Spin-orbit coupling proximity effect in MoS₂/Fe₃GeTe₂ heterostructures, *Applied Physics Letters* **120** (2022).
 - [49] C. Kittel and P. McEuen, *Introduction to solid state physics* (John Wiley & Sons, 2018).
 - [50] K. Momma and F. Izumi, VESTA 3 for three-dimensional visualization of crystal, volumetric and morphology data, *Journal of applied crystallography* **44**, 1272 (2011).
 - [51] S. Pal, K. Kumar, A. Banerjee, S. Roy, and A. Nigam, Non-equilibrium magnetic response of canonical spin glass and magnetic glass, *Journal of Physics: Condensed Matter* **33**, 025801 (2020).
 - [52] S. N. Kajale, J. Hanna, K. Jang, and D. Sarkar, Two-dimensional magnetic materials for spintronic applications, *Nano Research* **17**, 743 (2024).
 - [53] Y. Huang, X. Yao, F. Qi, W. Shen, and G. Cao, Anomalous resistivity upturn in the van der waals ferromagnet Fe₅GeTe₂, *Applied Physics Letters* **121** (2022).
 - [54] L. Du, J. Tang, Y. Zhao, X. Li, R. Yang, X. Hu, X. Bai, X. Wang, K. Watanabe, T. Taniguchi, *et al.*, Lattice dynamics, phonon chirality, and spin-phonon coupling in 2d itinerant ferromagnet fe₃gete₂, *Advanced Functional Materials* **29**, 1904734 (2019).
 - [55] N. J. Mosey, P. Liao, and E. A. Carter, Rotationally invariant ab initio evaluation of coulomb and exchange parameters for dft+u calculations, *The Journal of chemical physics* **129** (2008).
 - [56] W. Greiner, L. Neise, and H. Stöcker, The models of ising and heisenberg, in *Thermodynamics and Statistical Mechanics* (Springer, 1995) pp. 436–456.